Single electron dynamics

Toshimasa Fujisawa

NTT Basic Research Laboratories, NTT Corporation,
3-1 Morinosato-Wakamiya, Atsugi, 243-0198, Japan

CONTENTS

1. INTRODUCTION TO SINGLE-ELECTRON DYNAMICS

Electrical current is microscopically a flow of large numbers of electrons, each of which carries an elementary charge, e. For instance, one ampere corresponds to a flow of approximately 10^{19} electrons per second. We generally do not care much about the transport of each electron for such a large current. However, as the electrical current becomes smaller and smaller, the flow of individual electrons becomes important. A commercially available current meter can measure down to a few fA (noise floor of a few fA/$\sqrt{Hz}$), which corresponds to about 10^4 electrons per second. Usually, we cannot observe the flow of individual electrons in an electrical conductor. However, recent developments in nanotechnology allow us to control and measure single electron transport very accurately. An electron pump device, which carries exactly one electron during one cycle of voltage modulation, is considered a possible current standard with extremely high accuracy. A single-electron transistor has an extremely high charge sensitivity (about 10^{-5} electrons/$\sqrt{Hz}$) on a small conductive island. This device would detect individual electron transport of a current on the order of a few nA. With these techniques, various dynamical behaviors of single-electron can also be studied. Usually each electron moves randomly in a conductor. However, electron transport through a small conductive island, known as single electron tunneling, can be somewhat correlated. An electron that has entered the small island leaves it before another electron is allowed to enter. Moreover, in a one-dimensional array of small islands, each electron is expected to transport more regularly. This research on single-electron transport has been started by understanding the dc and low-frequency transport characteristics, but now they are moving to more high-frequency dynamical single-electron transport characteristics, which we call *single-electron dynamics*.

Another important aspect of a single electron is that its behavior is governed by quantum mechanics. One of the non-classical characteristics is the particle-wave duality. Although a single electron is a particle located somewhere when it is measured, it can behave as if it was located in two (or more) different places at one time. For instance, when an electron (the same is true for a photon or other single particles) is transmitted through

and diffracted from a pair of small holes (double slit), it appears randomly at a position on the screen behind the double slit. The probability of the appearance on the screen shows an interference pattern that is described by the wave characteristics of an electron (the quantum mechanical picture of an electron). One cannot determine the path (slit) an electron has taken without causing the interference pattern to disappear. This is an example of spatial interference, but similar interference can also appear in the time domain. Consider two conductive islands (double quantum dot) located close to each other. When an electron is added to this double dot system, it occupies one of the two dots in the classical picture. However, quantum mechanics allows it to occupy both dots simultaneously. One cannot determine which dot the electron occupies at a given time, but one can determine the probability of finding the electron in each dot. When an appropriate electromagnetic field is applied to the system, the probability starts to oscillate. This *coherent dynamics of single electron* is another interesting topic covered in this chapter.

A single electron rotates by itself (electron spin). Electron spin usually does not play an important role in non-magnetic materials. However, it can determine the transport characteristics of a small island (quantum dot) that contains a small number of electrons. Coulomb interactions of electrons confined in a small region induce different spin states, which give rise to spin-dependent transport. Single electron spin in a quantum dot shows a long energy relaxation time, and is expected to have a long decoherence time, which promises to provide the *coherent dynamics of single electron spin*.

One challenging research on coherent single-electron dynamics is to realize quantum computing hardware, in which information processing is performed in the time-evolution of quantum states. Quantum computing is expected to perform some sorts of calculations efficiently at amazing speed that is unavailable in a classical computing scheme. The single-electron charge state and the single-electron spin state in quantum dots are good candidates for basic building blocks of a quantum computer.

2. STATIC CHARACTERISTICS OF A SINGLE ELECTRON

A *small conductive island* that accommodates a tunable number of electrons is often used to manipulate a single electron [1]. The number of electrons in the island can be controlled one by one. When the island is so small that the energy quantization is significant, the island is often called a *quantum dot* [2]. Electrons occupy discrete levels, each of which has two-fold spin degeneracy. When a few electrons are confined in a well-defined potential, the quantum dot is often referred to as an *artificial atom*. Electrons occupy well-defined orbitals, as in a normal atom.

These islands, quantum dots, and artificial atoms are usually connected to the source and drain electrodes through tunneling barriers to allow transport measurements. A couple of gate electrodes are also used to control the electrostatic potential of the island and the tunneling barriers. In this section, we summarize the fabrication techniques of the devices and their dc transport characteristics.

2.1 Fabrication techniques

The fabrication techniques for single-electron devices have been developed together with large-scale integration technology for solid-state devices. Electron beam lithography, which patterns arbitrary fine structures with few nanometer resolution, is often used to fabricate small structures. Here, some typical fabrication processes are summarized.

Well-controllable quantum dots are often fabricated from two-dimensional electron gas (2DEG) formed in a modulation-doped heterostructure [3, 4]. The heterostructure consists of a thick high-quality undoped GaAs layer, an undoped $Al_xGa_{1-x}As$ layer (Al content of $x \sim 0.3$), and a Si-doped $Al_xGa_{1-x}As$ layer. The 2DEG accumulates at the interface of the GaAs and AlGaAs layers. Since the 2DEG is spatially separated from the doping layer, it shows a high electron mobility of 10^5 - 10^7 cm^2/Vs with typical sheet carrier concentration of n = 2 - 5×10^{11} cm^{-2} at low temperature (< 4 K). The quality of the 2DEG has been improved for its application to high-electron mobility transistors (HEMTs) as well as for physical interest in integer and fractional quantum Hall effects. Small structures, like quantum dots, can be fabricated by processing the heterostructure. For a typical fabrication procedure, the first step is a wet etching process for device isolation and to define a conductive channel. Next, some Ohmic contacts (AuGeNi alloy) are fabricated by metal evaporation, which is followed by a thermal annealing process. Then, fine Schottky gates (Au/Ti) are evaporated on the surface with the aid of electron beam lithography. Additional etching processes using a fine electron-beam lithographic pattern can define the conductive channel more precisely. Considering that the 2DEG is depleted approximately 50 - 200 nm away from the edge of the etched pattern and about 10 - 20 nm away from the moderately biased gate electrode, a small conductive island (quantum dot) of 100 - 1000 nm in size can be routinely fabricated. This technique provides high-quality nanostructures with multiple gates.

Extremely clean quantum dots containing a very few electrons have been fabricated in a pillar structure of a resonant tunneling heterostructure [5]. An undoped InGaAs potential well separated from n-type GaAs electrodes by AlGaAs tunneling barriers can be designed to accommodate 2DEG in the even at zero voltage. A pillar structure with diameter of $\sim$0.5 μm and height of $\sim$0.5

μm is patterned and fabricated by using electron-beam lithography and dry and wet etching. Then a gate electrode is deposited around the pillar structure. Electrons flow from the top of the pillar to the bottom of the structure. The electrons are confined in a square well potential in the vertical direction, and in a two-dimensional harmonic potential in the lateral direction. The advantage of this structure is that the electron number can be reduced completely zero. Since the confinement potential is well defined, the electronic state in the quantum dot can be predicted from the theoretical calculations.

Another fabrication process often used for superconductor and normal metal islands is shadow evaporation [6, 7]. By using a double (or triple) layer of resists having different sensitivities for electron beam lithography, suspended or overhanging resist layers can be fabricated. Then metals are evaporated from different angles to the sample to form multiple metal layers that overlap in some regions. A thin insulating layer can be inserted between metal layers by using an oxidation process. For example, two aluminum evaporations with oxidation in between provide $Al/AlO_2/Al$ tunneling junctions. Small metal islands, tunneling barriers, gate electrodes, and source and drain leads can be fabricated on a substrate by properly designing the lithographic pattern. High-quality Al islands show superconducting characteristics at low temperature and in a low magnetic field.

Much smaller islands, or quantum dots, can be fabricated by using various nanotechnologies. For instance, crystal growth of thin InAs on GaAs substrate results in the formation of nanometer-scale islands (10 - 50 nm). This is known as the Stranski-Krastanov growth mode, which occurs when there is large difference in the crystal lattice constants. Source and drain electrodes, as well as gate electrodes, can also be fabricated for transport measurements [8]. Moreover, a variety of materials, such as nano-particles of magnetic, superconductor, and semiconductor materials as well as molecules of carbon nanotubes and fullerenes, can also be used as small quantum dots. However, as the islands becomes smaller, fabrication processes for transport measurement generally become difficult.

Generally, larger quantum dots have smaller characteristic energies, and work only at lower temperatures. However, they can be fabricated together with multiple gate electrodes to control the characteristics of the dot independently. Therefore, the fundamental characteristics of quantum dots are investigated in relatively large quantum dots at very low temperature (< 0.1 K), while better characteristics are obtained in smaller quantum dots.

2.2 Coulomb blockade and single electron tunneling

Here we discuss how an electron can be manipulated in a small island. Consider a conductive island connected to the source and drain electrodes via tunneling barriers and connected to a gate electrode with a small capacitor, as schematically shown in Fig. 1(a) and in the equivalent circuit diagram of Fig. 1(b). We introduce the orthodox Coulomb blockade theory, which describes the Coulomb blockade (CB) effect and single electron tunneling (SET) behavior [1]. For simplicity we assume zero bias voltage is applied between the source and drain electrodes, $V_{SD} = 0$. The total energy, $U(N)$, of the system, in which an island containing N electrons is affected by a gate voltage, V_g, via a capacitance, C_g, is given by [9]

$$U(N) = \frac{(-Ne + C_g V_g + q_0)^2}{2C_\Sigma} + E_{int}(N). \qquad (1)$$

The first term is the electrostatic energy approximated by the constant capacitance model, i.e., constant Coulomb interaction in the island. Inside the parenthesis is the sum of the electron charge on the dot, the induced charge by the gate, and an offset charge, q_0. C_Σ is the total capacitance of the dot. The second term, $E_{int}(N)$, is the sum of the energies of the N occupied electron levels, measured relative to the Fermi energy of the leads, accounting for the internal degrees of freedom of the QD. Other corrections to many-body interactions can be included in E_{int}. We neglect the second term in this subsection, but discuss it in detail in the next subsection. Ignoring this term corresponds to considering a relatively large island containing many electrons that occupy continuum density of states. Even if an electron is excited to a higher energy state, the electron can relax quickly to the minimum energy, $E_{int}^{(\min)}$, which is almost independent of N.

Therefore, by neglecting E_{int}, the total energy of the system changes with V_g as shown in Fig. 1(c). The number of electrons, N, is determined to minimize the total energy and therefore becomes a well defined integer ($N = N_0,\ N_0 + 1,\ N_0 + 2,\ ...$). The energy gap to neighbor charge states can be maximized to $e^2/2C_\Sigma$, for instance, at $V_g = V_{g0}$. When excitation energies, such as the thermal energy, are much smaller than this energy, an electron can neither enter nor leave the island. Therefore, transport through the island is blocked (Coulomb blockade). The energy gap can be made zero by adjusting the gate voltage at $V_g = V_{g1}$, where N can fluctuate between N_0 and $N_0 + 1$ only by one, but not more than one. This means that electrons tunnel through the island one by one. This single electron tunneling scheme is maintained unless the excitation energy exceeds the charging energy, $E_c \equiv e^2/C_\Sigma$. The Coulomb blockade and single electron tunneling appear alternately by sweeping the gate voltage with a period given by e/C_g (CB oscillation).

When the source-drain voltage, V_{SD}, is applied, the CB region shrinks and the SET region expands as shown in the charging diagram of Fig. 1(d). The maximum width of a CB diamond region is given by E_c/e in the V_{SD} direction and e/C_g in the V_g direction. The CB and SET appear in diamond (parallelogram) regions as

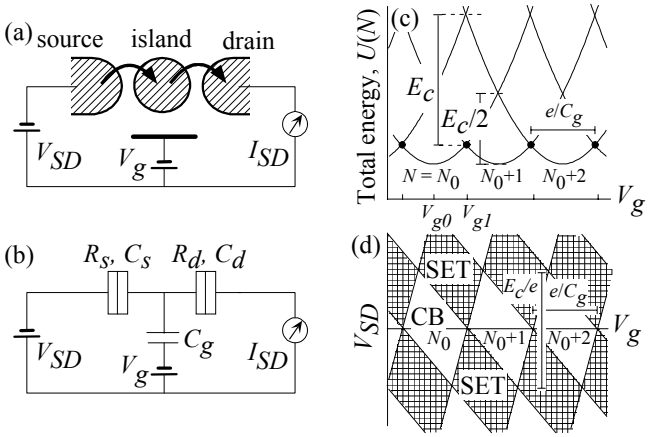

FIG. 1: Coulomb blockade (CB) and single electron tunneling (SET) in a single island. (a) Schematic diagram of the conductive region of a typical SET device (hatched regions). (b) Corresponding circuit diagram. The island is connected to the source and the drain via tunneling barriers, and is connected to the gate electrode by a capacitor. (c) Total energy, $U(N)$, of the system as a function of the gate voltage, V_g. (d) The diagram of the CB and SET regions in the $V_g - V_{SD}$ plane. Slightly asymmetric tunneling capacitances are assumed.

shown in Fig. 1(d). The number of electrons in the dot, N, can be controlled by changing V_{SD} or V_g.

2.3 Energy quantization and many-body effects

When the size of an island (quantum dot) is so small that an electron wave can interfere, only the constructively interfering wave (electron orbital) can exist in the quantum dot, forming quantized energy levels [2, 10]. Each level can accommodate two electrons with spin-up and spin-down. In a very simple picture, electrons occupy levels starting from the lowest, and making spin pairs. Therefore, the total spin, S, of the system is 0 for even N and 1/2 for odd N. $E_{int}(N)$ in Eq. 1 is the sum of the occupied energy levels for all N electrons. For this quantum dot regime, the characteristic energy for CB and SET is the addition energy, E_{add}, which is the energy required to add one electron to the quantum dot. When an electron is added to an odd-N quantum dot, the addition energy is identical to the charging energy, $E_{add}(\text{odd-}N) = E_c$. However, when an electron is added to an even-N quantum dot, excess energy equivalent to the energy spacing, Δ, between quantized levels is required, $E_{add}(\text{even-}N) = E_c + \Delta$. The difference in the addition energy is reflected in the width of CB regions, which now show even-odd asymmetry (wider width for even N).

However, when N is relatively small, electrons in a quantum dot interact, and the width of the CB region exhibits more complicated variations with N. This comes from the Coulomb interactions between the electrons in a quantum dot. Electrons occupy different orbitals that have different spatial distributions in the dot. Electrons prefer to occupy different orbitals in order to reduce Coulomb repulsion (the direct Coulomb interaction). Two electrons occupy different orbitals, rather than make a spin pair, if the energy gain is larger than the energy cost for taking a higher-energy orbital. If electrons occupy different orbitals, their spins prefer to maximize the total spin in order to gain the exchange Coulomb energy. These Coulomb interactions determine the electron filling in a quantum dot (many-body effects). The width of CB regions changes with N in a complicated manner. In other words, one can study the many-body effects from the N-dependent addition energy.

The many-body effects can be clearly studied in a quantum-dot disk, in which electrons are confined in a two-dimensional harmonic potential [10–12]. In this case, the orbitals can be expressed analytically, and can be identified as 1s, 2p, 3s and 3d, ... from the lowest energy to higher energy. Such a quantum dot is referred to as an artificial atom. The ground state of the one electron quantum dot (artificial hydrogen atom) is one electron in the 1s orbital. This configuration does not change with the magnetic field. However, the ground state of the two electron quantum dot (artificial helium atom) is the spin-singlet state having two anti-parallel-spin electrons in the 1s orbital, or the spin-triplet state having parallel-spin electrons in the 1s and 2p orbitals, depending on the strength of the Coulomb interactions and the level spacing. The transition from the spin-singlet state to the spin triplet state occurs by applying a magnetic field (B = 2 - 6 T), which increases the Coulomb interactions and decreases the level spacing. Note that similar singlet-triplet transition in a normal helium atom is expected to occur at an extremely high magnetic field of 4×10^5 T. One can study simple atomic physics in moderate parameter spaces using an artificial atom (see Sec. 3.10).

2.4 Double quantum dot

A double quantum dot comprises two quantum dots separated by a tunneling barrier[13–16]. If a quantum dot is an artificial atom, a double quantum dot can be regarded as an artificial diatomic molecule. The two quantum dots can be coupled electrostatically (ionic bond in the language of chemistry) as well as quantum mechanically (covalent bond). Consider two quantum dots connected through a tunneling barrier with a capacitor, C_c, and tunneling coupling, T_c. Figure 2(a) is the schematic diagram of the double dot connected between the source and drain in series. For a moment, we neglect the effect of the source and drain contacts for simplicity. Figures

2(b) - 2(d) show the charging diagram of the double quantum dot in different regimes [14]. The gate voltages, V_{gl} and V_{gr}, are swept to shift the potential of the respective dots. (n, m) represents the stable charge state in which n and m electrons occupy the left and the right dot, respectively. When there are no interactions between the two dots ($C_c \sim 0$ and $T_c \sim 0$), the charging diagram is just Coulomb blockade oscillations of the two dots [See Fig. 2(b)]. If only the electrostatic coupling is turned on, ($C_c > 0$, $T_c \sim 0$), charging of an electron on one quantum dot lifts up the potential of the other dot. And the gate voltage for one dot also affects the potential of the other dot via the coupling capacitor. In this case, the charging diagram becomes a hexagonal honeycomb structure as shown in Fig. 2(c). Each crossing point in Fig. 2(b) splits into two triple points [See E and H in Fig. 2(c)], whose spacing corresponds to the inter-dot coupling energy defined by

$$E_{id} = e^2 C_c / C_{\Sigma l} C_{\Sigma r}. \tag{2}$$

Here $C_{\Sigma l}$ and $C_{\Sigma r}$ are the total capacitance of the left and the right dot, respectively. The transport through the double dot from the source to the drain is allowed only at these triple points, where three charge states are energetically degenerated. At the triple point indicated by E, an electron tunnels from the left to the right (the clockwise direction in the charging diagram) or the right to the left (the counter clockwise direction) sequentially. However, the tunneling sequence at the triple point H is somewhat peculiar. The electron tunneling process propagates in the reverse direction of the electron flow. It is easy to conceive that a hole, rather than an electron, tunnels sequentially.

Now we discuss the amplitude of current through a double quantum dot. We assume that electrons can tunnel between the two dots elastically, i.e., only when the discrete energy states of the two quantum dots are aligned approximately within the lifetime broadening of the states. Then we expect a very sharp peak at the resonance, whose current profile is basically independent of the thermal distributions in the leads. In the vicinity of a triple point, only one energy state in each dot contributes to the transport [17]. At a large source-drain voltage, which saturates the current, the current profile is determined by the energy difference between the two charge states, ε. And it is given by a Lorentzian function as

$$I(\varepsilon) = \frac{e}{\hbar} \frac{\Gamma_o T_c^2}{\varepsilon^2 + \Gamma_o^2/4 + T_c^2(1 + \Gamma_o/\Gamma_i)}, \tag{3}$$

where Γ_i and Γ_o are the tunneling rate of the incoming and outgoing barriers, respectively [15]. Note that Γ_i and Γ_o appear asymmetrically, so the three parameters, T_c, Γ_i, and Γ_o, can be deduced from the current profiles obtained at different current directions. This is a convenient way to determine the parameters experimentally, if the inelastic current (see Sec. 3.11) and other currents from excited states can be neglected.

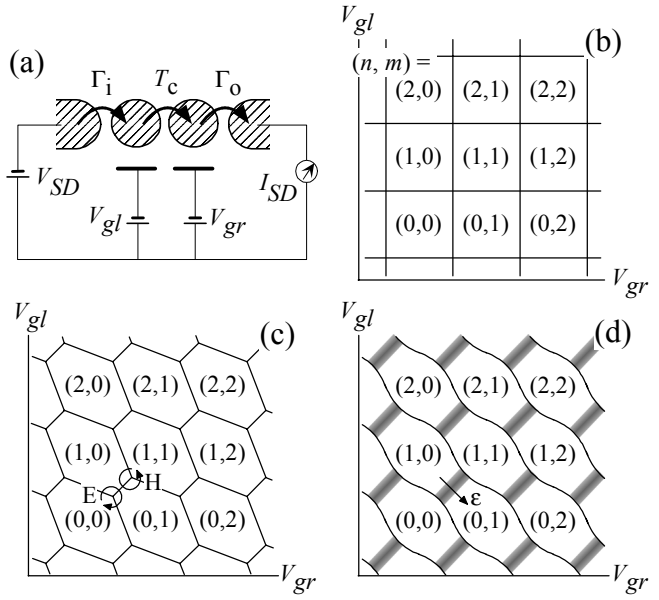

FIG. 2: Charging diagram of a double quantum dot. (a) Schematic circuit diagram of a double dot. (b-d) Charging diagrams in the different regimes. (a) Both electrostatic and tunneling couplings are neglected. (c) Only the electrostatic coupling is considered. Single electron transport through the double dot with electron-like process at the triple point, E, and with hole-like process at H. Circled arrows are typical gate-voltage trajectories in the single-electron pumping operation. (d) Both electrostatic and tunneling couplings are considered. The charge state is no longer a good quantum state in the hatched regions.

If the tunneling coupling, T_c, is made larger than Γ_i, and Γ_o, coherent tunneling coupling (covalent bond) between the two dots is expected [14, 18, 19]. The charging diagram deforms as shown in Fig. 2(d). In the gray regions, one cannot distinguish whether a single electron is in the left or right dot. The localized states in each dot are mixed into bonding and anti-bonding states, which are energetically separated by $2\hbar T_c$ at the original triple points. The current peak is broadened and elongated into a crescent shape in the vicinity of the original triple point. Finally, if the tunneling coupling becomes too strong, the double dot becomes effectively a large single dot, in which just single CB oscillations are expected. In the intermediate and intriguing coupling regime, two dots are coupled strongly and coherently, but are weakly coupled to the source and drain electrodes just to measure the current. This double dot can be considered a tunable two-level system, which is discussed in the next subsection.

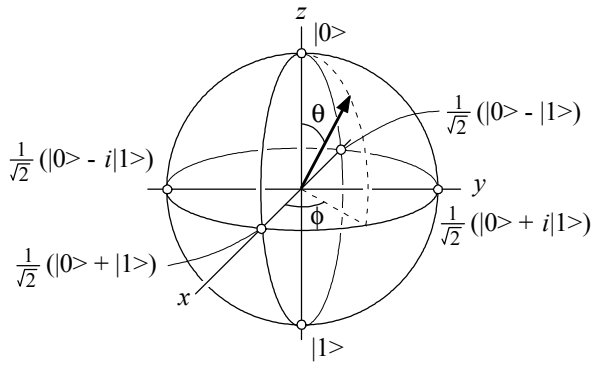

FIG. 3: Bloch sphere of a spin-1/2 system. Any two-level system can be mapped onto the Bloch sphere. The arrow, θ and ϕ in the polar coordinate, indicates the state, $|\psi\rangle = \cos\frac{\theta}{2}|0\rangle + e^{i\varphi}\sin\frac{\theta}{2}|1\rangle$.

2.5 Two-level systems - electron-spin and pseudo-spin -

The two-level system is the simplest system in which quantum mechanical characteristics can appear, and provides an important model for the study of the quantum dynamics. After describing a single electron spin as a typical two-level system, we define a tunable two-level system in a double quantum dot.

An electron spin is fully described by quantum mechanics. The direction of an electron spin can be arbitrary in principle. However, electron spin takes spin-up, denoted here by $|0\rangle$, or spin-down, $|1\rangle$, when the z-component of the spin is measured. An arbitrary spin state before the measurement is described by a linear superposition of these two states (bases) as

$$|\psi\rangle = \cos\tfrac{\theta}{2}|0\rangle + e^{i\varphi}\sin\tfrac{\theta}{2}|1\rangle, \tag{4}$$

where θ and φ are mixing angles that determine the probability of measurement results. This representation is chosen to point the spin orientation in spherical coordinate, and it is convenient for describing the state in the Bloch sphere of Fig. 3.

Now, consider an electron spin in the presence of magnetic field $B = (B_x, B_y, B_z)$. The Hamiltonian of the system can be described as

$$H = -\tfrac{1}{2}\mu_s(\sigma_x B_x + \sigma_y B_y + \sigma_z B_z), \tag{5}$$

where σ_x, σ_y, and σ_z are the Pauli matrices, and μ_s is the magnetic moment of a spin. The stationary eigenstates of the system can be obtained by solving the time-independent Schrödinger equation, $H|\psi\rangle = E|\psi\rangle$. This gives the eigen energies

$$E_\pm = \pm\tfrac{1}{2}\mu_s\sqrt{B_x^2 + B_y^2 + B_z^2} \tag{6}$$

and the corresponding eigenstates of

$$|\psi_+\rangle = \sin\tfrac{\theta}{2}|0\rangle - e^{i\varphi}\cos\tfrac{\theta}{2}|1\rangle, \tag{7}$$

$$|\psi_-\rangle = \cos\tfrac{\theta}{2}|0\rangle + e^{i\varphi}\sin\tfrac{\theta}{2}|1\rangle, \tag{8}$$

where θ and φ are the directions of the magnetic field. This argument looks roundabout, since the z-direction may be chosen as the direction of the magnetic field for simplicity. However, Eqs. 6 and 7 give general eigenstates for any two-level system under a Hamiltonian, which can be expressed by fictitious magnetic fields (Eq. 5).

Now, we define a two-level system in a double quantum dot [16, 18]. We choose the ground state of the charge state $(1,0)$ as one state $|0\rangle$, and the ground state of the charge state $(0,1)$ as the other state $|1\rangle$. Other excited states and other charge states can be ignored, if they are energetically much higher than the lowest two energy states, $|0\rangle$ and $|1\rangle$, i.e., if the double quantum dot is properly adjusted somewhere in between a pair of triple points [gray regions in Fig. 2(d)]. In addition, the double dot can be effectively isolated from the source and drain electrodes because the inter-dot charging energy can block the transport (See Sec. 2.4). The energy difference, ε, between the two states can be changed by the gate voltages as shown by the arrow in Fig. 2(d). The coherent tunneling coupling, T_c, allows the system to change between $|0\rangle$ and $|1\rangle$. In this case, the Hamiltonian of the system is written as

$$H = \tfrac{1}{2}\varepsilon\sigma_z + \hbar T_c\sigma_x, \tag{9}$$

where $\frac{1}{2}\varepsilon$ and $\hbar T_c$ can be regarded as fictitious magnetic fields in the z and x directions, respectively (Compare with Eq. 5). Therefore, we can map the two-level system of the double quantum dot onto the spin system (pseudo-spin model). Similarly any two-level system can be mapped onto the spin system, and its superposition can be represented in the Bloch sphere. The eigen energies of the double quantum dot are given by

$$E_\pm = \pm\tfrac{1}{2}\sqrt{\varepsilon^2 + 4(\hbar T_c)^2}, \tag{10}$$

which is schematically shown in Fig. 4(a) [18]. The corresponding wavefunctions, which are schematically shown in Figs. 4(b)-(d), are symmetric for energy E_- (often called the symmetric state or bonding state), and anti-symmetric for energy E_+ (anti-symmetric state or anti-bonding state). And the eigenstates are always in the x-z plane ($y = 0$) of the Bloch sphere.

3. SINGLE-ELECTRON DYNAMICS IN NANOSTRUCTURES

In this section, we discuss the dynamical behavior of a single electron. In most of the phenomena, various types

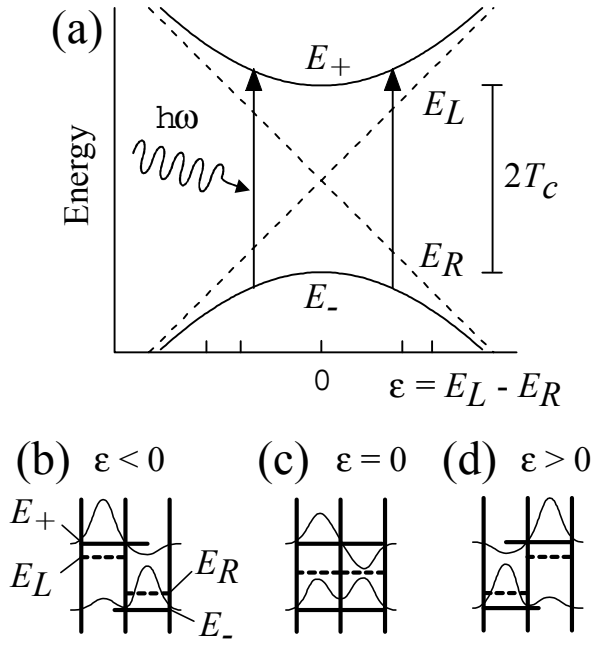

FIG. 4: (a) Schematic energy diagram of a double quantum dot. E_L and E_R are the energies of the localized charge state $(1,0)$ and $(0,1)$, respectively. When the tunneling coupling is turned on, the bonding state with the energy E_- and the anti-bonding state with the energy E_+ are formed. (b - d) Schematic energy diagram and wavefunctions of the bonding and anti-bonding states for (b) $\varepsilon < 0$, (c) $\varepsilon = 0$, and (d) $\varepsilon > 0$.

of potential modulations are included in the discussion of time-integrated tunneling current. When the modulation is relatively slow as compared to the tunneling rate, the system changes adiabatically. We can still use the stationary states of quantum dots in the absence of the modulation. However, if the modulation frequency becomes higher than the tunneling rate, the system changes non-adiabatically, and the state is no longer the original stationary state. We have to use time-dependent Schrödinger equations, $i\hbar d\psi/dt = H\psi$, to describe the dynamics. This section also describes the decoherence mechanisms, which are very important characteristics in the dynamics. Finally, measurement techniques for single electron states in a relatively short time domain are discussed.

3.1 Single-electron turnstile and pump

Single-electron turnstiles and pumps are single-electron devices that carry exactly one electron from one electrode (the source) to the other electrode (the drain) during one cycle of the periodic potential modulation [20]. During the first half of the modulation period one electron tunnels from the source to the island, and the electron tunnels out to the drain during the second half of the cycle. By repeating the modulation at a sufficiently high frequency, typically $f \sim 10$ MHz, a reasonable electrical current, $I = ef \sim 1.6$ pA, is obtained. These devices have been discussed as a possible current standard for metrology [21]. The frequency locked current in a single electron pump, the frequency-locked voltage generated by Josephson effect, and the quantum resistance realized by the quantum Hall effect are expected to close the quantum metrology triangle formed by voltage, current, and frequency.

Current in a turnstile device is driven by an external dc bias voltage applied between the source and drain, and the current is regulated so that only one electron is allowed to pass through the device during one cycle [22]. The current direction is given by the polarity of the bias voltage, and the current vanishes at zero bias voltage. On the other hand, the current in single-electron pumps is generated by a pumping process from the source to the drain. The direction of the pumping current is independent of the applied bias voltage, and it works even at zero bias voltage [23]. Usually, the turnstile devices are operated with a single modulation voltage, while the pump devices are operated with more than two gate voltages modulated with different phases.

Consider pumping processes in a double quantum dot. The charge state of a double quantum dot is represented by (n,m), where n and m are the number of excess electrons in the double dot [See Fig. 2(c)]. If the system is initially in the $(0,0)$ state, modulation voltages are designed to move the charge state to the $(1,0)$ state, followed by the $(0,1)$ state, and return it to the initial state $(0,0)$. During this cycle, an electron moves from the left to the right sequentially. This trajectory is schematically shown by an arrow enclosing the triple point E in Fig. 2(c). The other trajectory in the reversed direction enclosing the other triple point H carries a hole (0 state) from the right to the left, which gives the same current direction. In this way, exactly one electron, or hole, is carried from one lead to the other in one cycle of the potential modulation.

For metrology, an extremely high accuracy of less than 10^{-8} errors per cycle is required. The deviation from the frequency-locked current arises from thermal activation, Poisson tunneling statistics, the co-tunneling process, and so on. The probability of thermal excitation to other charge states can be suppressed below 10^{-8} at a dilution-refrigerator temperature of less than 50 mK for a typical double dot with inter-dot charging energy of about 100 μeV [20]. The current error also arises from the Poisson statistics of tunneling events, whose interval is widely distributed. Even when an electron is allowed to tunnel, the tunneling may not happen during the finite period of the cycle. This error can be reduced by making the modulation frequency much smaller than the tunneling rate of the barriers.

The co-tunneling process, which is the simultaneous

tunneling over two (or more) tunneling junctions via an intermediate virtual state [24], is a serious problem. The co-tunneling current survives even at zero temperature. Although the co-tunneling current is much smaller than the frequency-locked current, co-tunneling can easily degrade the accuracy of the current standard, especially when higher current is required. The co-tunneling current can be reduced either by driving the pumping device with a high resistor located very close to the device, or by using multiple tunneling junctions connected in series.

Other practical problems arise from low-frequency electrical noise and background charge fluctuations, which shift the effective operating gate voltage randomly, and high-frequency (microwave to far-infrared region) noise, which gives rise to photon-assisted tunneling processes [25]. By adjusting the operating parameters properly, a single-electron pump with seven tunneling junctions works very nicely with an error per pumped electron of $1.5\text{x}10^{-8}$ [26]. Single-electron pumps provide extremely accurate current of the order of $\sim$1 pA. Another way to achieve a possible current standard at a relatively large current is the moving quantum dot, which is discussed in Sec. 3.3.

The single electron pump is a fundamental tool that allows us to manipulate electrons one by one. In principle, one can design the voltage waveform so that a single electron is injected into or extracted from an island *on demand* within the accuracy of the inverse of the tunneling rate. One can add any operation or manipulation during the interval.

3.2 Single electron tunneling oscillation

Single electron tunneling, in which electrons travel through an island one by one, is a sort of correlated tunneling process over the two junctions. In normal SET devices, tunneling events are uncorrelated *in time*, and the interval between them is distributed according to Poisson statistics. However, the distribution of the tunneling interval can be made narrower than Poisson statistics (sub-Poisson statistics), and each electron tunneling can take place more regularly (SET oscillation).

A very simple scheme for SET oscillation is a small tunneling junction driven by a constant current. When the tunnel junction with a small tunneling capacitance is driven by a small constant current, the voltage across the junction increases linearly in time due to the charging. Single electron tunneling is allowed only when the voltage exceeds the charging energy of the junction, and the voltage drops suddenly by discharging (tunneling of) an electron. Therefore, the voltage across the junction shows a saw-tooth pattern in time. The charging and discharging should take place almost regularly as long as the junction is driven by a constant current. The constant current source can in principle be generated by a high-resistance resistor connected to the junction [27, 28]. However, it is not easy to fabricate such a resistor. A small parasitic capacitor in the vicinity of the junction smears the saw-tooth pattern of the voltage difference, and the junction is then effectively driven by a constant voltage.

Another way to achieve SET oscillation is a one-dimensional array of small islands connected by tunneling barriers. When an excess electron is injected into the array, potential distribution inside the array shows soliton characteristics (charge soliton). The soliton has a characteristic size, $M \sim \sqrt{C_T/C_0}$, in unit of an island, where C_T and C_0 are the tunneling capacitance and the self-capacitance of an island, respectively. If the length of the array is longer than $2M$, transport through it is influenced by Coulomb repulsion between the solitons. The solitons line up in a Wigner lattice inside the array, and propagate in a regular way (SET oscillation). This type of SET oscillation has been indirectly observed under microwave irradiation, where the SET oscillation is locked at the applied frequency [29]. The appearance of non-linear characteristics under microwave irradiation indicates correlated transport in the one-dimensional array of islands.

The correlated tunneling process can also be studied in the shot noise of the single electron tunneling current. When the current is carried by a Poisson process, the shot noise is given by $2e|I|$ (full shot noise), where I is the current. The suppression from the full shot noise indicates time-correlated tunneling and sub-Poissonian statistics. Even in a conventional single quantum dot device, the shot noise can be suppressed by half if the incoming and outgoing tunneling rates are almost the same [30, 31]. It is theoretically expected that shot noise in resonant Cooper pair tunneling can be suppressed significantly [32].

3.3 Moving quantum dots

In this subsection, we discuss the unique characteristics of moving quantum dots, in which an array of quantum dots each containing exactly one electron propagates from the source to the drain. When a high-frequency voltage (typically a few GHz) is applied to a metal electrode on a piezoelectric material (such as GaAs), a surface acoustic wave (SAW) is generated and propagates on the surface. The propagating SAW deforms the crystal lattice, thus modulating the conduction band in the vicinity of the surface through the piezoelectric interaction between the lattice deformation and the electrons. Therefore, a sinusoidal potential for electrons propagates with the SAW velocity, $v = 2980$ m/s for GaAs. When a one-dimensional channel is pre-fabricated along the SAW propagation direction by conventional lithographic techniques, a moving 1D array of potential puddles (quantum dots) is formed. Each quantum dot carries a well-defined integer number of electrons, n (= 1, 2, 3,...), which can be

tuned by external voltages or the intensity of the SAW. The acousto-electric current is quantized to $I = nef$ with the SAW frequency, f [33–37]. In this case, electrons are transferred with the propagating potential, and no tunneling processes are involved. The current amplitude can be on the order of nano-amperes (I $\sim$ 0.48 nA for $n = 1$ and $f = 3$ GHz), which is about three orders of magnitude larger than that in electron pump devices. Therefore, more practical current-standard devices are expected.

In order to obtain a sufficient potential modulation, the SAW is usually generated with a narrow-band interdigital transducer situated a few millimeters from the electrical channel [34]. The typical wavelength of the SAW is about 1 μm for $f_{SAW} = 3$ GHz, and should be comparable to the length of the one-dimensional channel. Application of a few milliwatts of microwave power to the transducer gives a typical potential modulation of about 1 meV in the active region. Note that the modulation amplitude is significantly reduced by the screening effect from the existing electrons.

The accuracy of the current is expected to be excellent (less than 10^{-10} errors for modulation amplitude of about 20 meV), when the electron transport is driven adiabatically [33, 38]. Practical error may come from insufficient potential modulation, background charge fluctuations, the existence of standing wave modes, thermal effects, and so on. Some devices show current accuracy of about 5×10^{-5} [35, 36], but this accuracy is not yet enough for metrology purposes. Further improvements are desired for this device.

3.4 Photon assisted tunneling

In the previous sections, the energy states in quantum dots are assumed to be shifted adiabatically in proportion to the applied modulation voltages. This is a good approximation, provided the modulation frequency is much lower than the tunneling rate. However, when the modulation frequency exceeds the tunneling rate, a quantum mechanical description of the system is required in order to understand the non-adiabatic transport characteristics. In this and the next few subsections, we concentrate on sinusoidal potential modulation, in which the modulation can be regarded as a coherent photon field. Various kinds of electron-photon interactions analogous to those in quantum optics are expected. For instance, electrons can tunnel through a barrier by absorbing or emitting a photon. This photon-assisted tunneling (PAT) has been theoretically developed in the Tien-Gordon theory [39, 40], and experimentally studied in the transport through Josephson junctions [41] and resonant tunneling structures [42, 43], as well as quantum dots [44, 45]. Coherent electron-photon coupling is expected, and has actually been demonstrated in double quantum dots and superconductor islands.

When a sinusoidal voltage, $V(t) = V_0 \sin\omega t$, is applied across a tunneling barrier, the wavefunction of an electron on one electrode acquires a phase shift, $\int eV(t)dt/\hbar$, relative to the other electrode. The wavefunction can be written as a superposition of a series of photon sidebands as

$$\psi(x,t) = \psi_0(x,t) \sum_{n=-\infty}^{\infty} J_n(\alpha) \exp(-in\omega t), \qquad (11)$$

where $J_n(\alpha)$ is the n-th order Bessel function of the first kind, $\alpha \equiv eV_0/\hbar\omega$ is the normalized modulation amplitude, and $\psi_0(x,t)$ is the original stationary wavefunction in the absence of sinusoidal voltage. The energies of the photon sidebands are separated by the photon energy $\hbar\omega$, and the amplitude of each wavefunction is proportional to $J_n(\alpha)$ [as shown schematically in the inset of Fig. 3(a)]. Therefore, the photon assisted tunneling can be considered as a normal tunneling process to one of the photon sidebands. The effective tunneling rate to the n-th sideband state is given by

$$\Gamma_n = J_n^2(\alpha)\Gamma, \qquad (12)$$

where Γ is the original tunneling rate in the absence of modulation. Here the energy dependence of Γ is neglected for simplicity. $n = \pm1, \pm2, ...$ corresponds to the tunneling with $|n|$-photons absorption (for positive n) and emission (for negative n). Equation 12 can also be applied in the case of intense microwaves, where nonlinear optical effects can appear. Figure 5(a) shows the function $J_n^2(\alpha)$, which indicates how the effective tunneling rate (or current) changes with the normalized modulation amplitude α. For a weak amplitude of $\alpha \ll 1$, Γ_n is proportional to the n-th power of the photon power, that is $J_n^2(\alpha) \sim (\alpha^2)^n$. For a strong amplitude of $\alpha \gtrsim 1$, however, $J_n^2(\alpha)$ is an oscillating function of α. At a specific amplitude where $J_1(\alpha) = 0$, for instance at $\alpha \sim 2.8$, tunneling through a one-photon sideband should vanish even in the presence of an intense oscillating potential. It should be noted that the zero-photon tunneling rate Γ_0 for $n = 0$ is also affected by the photon field, and the total sum is always conserved, $\sum_{n=-\infty}^{\infty} J_n^2(\alpha) \equiv 1$.

The Tien-Gordon theory explains very well the I-V characteristics of Josephson junctions and other tunneling devices like resonant tunneling structures and superlattices in the presence of microwaves, millimeter waves, THz waves, and far-infrared light [40–43]. Here we focus on the photon assisted tunneling in single-electron systems [44, 45]. A microwave (photon energy of 4 - 200 μeV for microwave frequency of 1 - 50 GHz) is often used as a coherent photon source. Application of a microwave on a gate or source-drain electrodes induces photon assisted tunneling on the two tunneling barriers. Since the two tunneling barriers are close to each other, it is technically difficult to control the modulation amplitude across

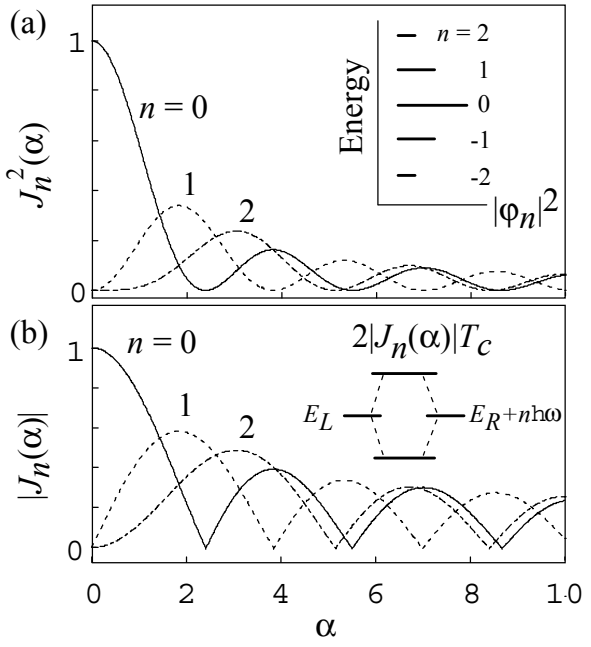

FIG. 5: (a) The square of the Bessel function. The photon-assisted tunneling current is proportional to the square of the Bessel function. The inset shows the sideband structure in the presence of oscillating potential. The length of the bars schematically indicates the amplitude of the wavefunctions. (b) The absolute value of the Bessel function. The energy splitting of the two states separated by n times the photon energy is proportional to the absolute value of the Bessel function.

each barrier independently, and photon-assisted tunneling can occur at either barriers. Nevertheless, the flow of current through the device can be quantitatively explained by the Tien-Gordon theory. The photon assisted tunneling from the continuum density of states in the electrode to a discrete energy state in the quantum dot produces a pumping current. A broad pumping current with a width corresponding to the photon energy appears in the vicinity of the SET current peak.

When a microwave is properly applied to modify the potential of the quantum dot, coherent tunneling through one of the photon sidebands is expected. An electron can tunnel into the dot by absorbing one photon through one barrier, and simultaneously tunnel out from the dot by emitting one photon through the other barrier. Distinct resonant PAT current peaks have been observed [46], indicating a coherent PAT process. In this case, the PAT current peaks are separated from the SET current peak by the photon energy. Furthermore, when the photon energy is made higher than the energy spacing in the quantum dot, one can excite an inner electron in the quantum dot to the reservoir. This process is analogous to the photo-ionization process of atoms.

3.5 PAT in a double quantum dot

A more interesting case is the electron-photon interaction in a double quantum dot, where an oscillating potential is applied between two discrete energy states [47, 48]. Note that a similar situation can be realized in a superconducting island, where photon assisted tunneling of a Cooper pair is observed between superconducting charge states in the island [49]. In this subsection, we restrict ourselves to a weakly coupled double dot, where an electron tunnels sequentially through three barriers. (See next subsection for strongly-coupled double dot.) In this case, we can still use the Tien-Gordon theory to describe the pumping current. The photon assisted tunneling current appears as a very sharp peak because of the discrete energy states. The peak appears when the two energy states are exactly separated by the photon energy. The current profile is given by Eq. 3 by substituting $J_n(\alpha)T_c$ for T_c [47]. In the weak coupling limit, the width of the peak is determined by the tunneling rate of outer barriers in principle, or by the effective electron temperature in some cases. In a low-temperature cryostat with a low-noise measurement system, the width can be reduced to a few μeV, corresponding to a frequency of about 1 GHz. The double dot is expected to act as a good microwave and millimeter wave spectrometer [50]. The current increases linearly with microwave power in the low-power limit, as expected from Eq. 12 [18, 51].

Furthermore, the double dot is a unique system in which population of each quantum dot can be controlled by external voltages [48]. In the normal population, the occupied state is energetically lower than the empty state, and excitation from the lower state to the higher state takes place by a photon absorption. However, in the *inverted population*, the occupied state has a higher energy than the empty state, and the microwave stimulates the transition from the higher state to the lower state by emitting a photon (*stimulated emission*). One can study microwave emission and absorption spectra just by changing the voltages.

3.6 Coherent electron-photon interaction

Here we discuss the coherent electron-photon interaction in a strongly-coupled double quantum dot, where the simple Tien-Gordon theory cannot be applied [52, 53]. In this case, the double dot can be considered as a two-level system. In order to generalize the problem, we use the pseudo-spin model introduced in Sec. 2.5. We consider that a microwave is applied to the two-level system to modify the energy difference, ε, between the two charge states, $(1,0)$, denoted by $|0\rangle$, and $(0,1)$, denoted by $|1\rangle$; $\varepsilon(t) = \varepsilon_0 + \varepsilon_1 \cos\omega t$. Then the Hamiltonian of the system is time-dependent and given by

$$H(t) = \tfrac{1}{2}(\varepsilon_0 + \varepsilon_1 \cos\omega t)\sigma_z + \hbar T_c \sigma_x, \qquad (13)$$

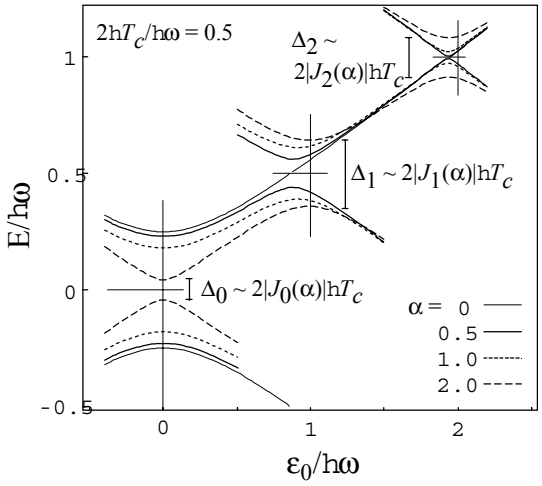

FIG. 6: Eigen energy, E, of the two-level system in a double quantum dot in the presence of microwave modulation. The numerical calculation is done for $2\hbar T_c/\hbar\omega = 0.5$ and $\alpha = \varepsilon_1/\hbar\omega = 0$, 0.5, 1, and 2.

where T_c is the tunneling coupling. When the Hamiltonian is periodic, $H(t+T) = H(t)$, with the period $T = 2\pi/\omega$, the eigenstates have the form $\psi(t) = e^{-iEt/\hbar}u(t)$, where E is the quasi-energy and $u(t)$ is a periodic function (Floquet function) with the period T. E and $u(t)$ are eigen-energy and eigen-state of the one-period evolution operator $U(T)$, which can be obtained by integrating the equation

$$i\hbar\frac{\partial}{\partial t}U(t) = H(t)U(t) \tag{14}$$

numerically [54].

Figure 6 shows the numerical calculation of the eigen-energy, E, for different normalized modulation amplitudes, $\alpha = \varepsilon_1/\hbar\omega$. The trace for $\alpha = 0$ is identical to that in Fig. 4(a), which schematically illustrates photon excitation from the bonding state (lower energy) to the anti-bonding state (higher energy). When the microwave amplitude is very weak, $\alpha \ll 1$, the application of the microwave does not perturb the energy states of the double dot. A current peak appears when the bonding and anti-bonding states are exactly separated by the photon energy, $\varepsilon = \sqrt{(\hbar\omega)^2 - 4(\hbar T_c)^2}$ [See arrows in Fig. 4(a)]. So there is a minimum frequency, T_c/π, to observe the microwave excitation current. This is an accurate measurement to experimentally determine ε and T_c, since it can be deduced from the frequency. Actually, the anti-crossing behavior has been demonstrated in a strongly coupled double dot and in a superconducting island [18, 49].

However, eigenstates of the system are influenced by microwave modulation, as shown in Fig. 6. As the amplitude increases, the original bonding and antibonding states, $|\psi_+\rangle$ and $|\psi_-\rangle$, are coherently coupled with the aid of n-photons, and a new energy gap, Δ_n, appears at the energy spacing close to the integer multiple of the photon energy, $\varepsilon_0 \sim n\hbar\omega$ [53]. The appearance of the gap indicates the coherency of the system, and the absorption and emission can take place coherently and oscillatory (Rabi oscillations, see next subsection). In the limit $T_c \ll \omega$, where analytical solutions can be obtained, the n-th energy gap, Δ_n, is approximately given by

$$\Delta_n = 2|J_n(\alpha)|\hbar T_c \tag{15}$$

at $\varepsilon_0 = n\hbar\omega$ [53]. Figure 4(b) shows the Bessel function, $|J_n(\alpha)|$, to illustrate how the energy gap changes with α [Compare with the square of the Bessel function for Tien-Gordon theory in Fig. 4(a)]. As is also seen in Fig. 6, the energy gaps change with α. It should be noted that the position of the gap also changes. The energy gap with one-photon appears at $\varepsilon = \pm\sqrt{(\hbar\omega)^2 - 4(\hbar T_c)^2}$, in the case of weak microwave amplitude, $\alpha \ll 1$, while it shifts toward $\varepsilon = \hbar\omega$ for strong amplitude. This shift is also observed as a shift of the current peak in a double quantum dot device [55]. Strong non-linear electron-photon coupling can be studied in quantum dot systems.

3.7 Coherent oscillations in the time domain

In this subsection, we discuss some coherent oscillations in the time domain. First, we describe Rabi oscillations in a double quantum dot under microwave irradiation. Then, a slightly different type of charge oscillation induced by abruptly changing a gate voltage, and spin rotation in the microwave magnetic field are discussed.

In order to simplify the problem, we consider that the two levels in the double quantum dot are separated by ε in the limit of $\hbar T_c \ll \varepsilon$ and the microwave is irradiated at the resonant condition, $\varepsilon = \hbar\omega$, with the same notations as in the previous subsection. Therefore, the localized state, in which an electron occupies the left or the right dot, gives a good picture of the system. Suppose an electron occupies the left dot before microwave irradiation at $t < 0$, and the microwave is turned on for the period, $0 < t < t_p$. If microwave absorption and emission take place coherently during the microwave irradiation, the probability of finding the electron in the dot should oscillate in time,

$$P_{l/r}(t) = \frac{1}{2}[1 \pm \cos(\Delta_1 t/\hbar)], \tag{16}$$

where the frequency, $\Delta_1/\hbar$, is given by Eq. 15. This is analogous to Rabi oscillations in atomic systems [56]. One cannot directly observe the oscillation by detecting the location of the electron, since the measurement itself causes the decoherence of the system and ceases the oscillation. Instead, one can measure the location of the electron after turning off the microwave at $t > t_p$. A simple measurement scheme is a current measurement.

The gate voltages can be adjusted so that an electron in the right dot, for example, can escape to the lead to measure as a current. This tunneling rate must be much smaller than the oscillation frequency to reduce the decoherence. However, this measurement yields only one electron at most per pulse. Since a typical current meter requires about 10^5 electrons to detect a signal, a reasonable current can be obtained by repeating identical measurements (microwave pulses) many times. Then, the current is proportional to the probability, $P_r(t_p)$. The oscillation pattern appears if the current is measured at various pulse lengths, t_p, or strengths of electron-photon coupling, $\Delta_1 = 2|J_1(\alpha)|\hbar T_c$.

Practically, the coherent oscillation does not continue forever due to dissipation and decoherence (Sec. 3.8), and ends up with a stationary ground state. In order to obtain the oscillations, higher oscillation frequency and less decoherence are required. However, the observation of Rabi oscillations in a single-electron system is difficult, because of technical difficulties in obtaining a short microwave pulse as compared to the relatively short decoherence time of single charge states. Successful oscillations have been observed in an exciton (electron-hole pair) system, in which ultrafast optical excitation are used [57].

A slightly modified technique is coherent charge oscillation induced by a high-speed voltage pulse, instead of a microwave pulse [58, 59]. A localized state is prepared before the pulse, and the two levels are aligned during the pulse ($\varepsilon = 0$) so that the electron can go back and forth between the two dots coherently.

Neglecting the source and drain electrodes, the Hamiltonian of the system, by using the same notation as in Sec. 2.5, changes from

$$H(t) = \tfrac{1}{2}\varepsilon_0\sigma_z + \hbar T_c\sigma_x \qquad (t < 0) \tag{17}$$

before the pulse, where $|\varepsilon_0| \gg T_c$ is chosen to give a localized state in the steady state, to

$$H(t) = \tfrac{1}{2}\varepsilon_1\sigma_z + \hbar T_c\sigma_x \qquad (0 < t < t_p) \tag{18}$$

during the pulse, where $\varepsilon_1 \sim 0$ is the situation we are interested in. The dynamics of the pseudo-spin can be understood well using the Bloch sphere introduced in Sec. 2.5. The system is initialized in the ground state of Eq. 17 [at the north pole in the Bloch sphere of Fig. 7(e)] at $t = 0$, and then precesses about the x-axis during the pulse. In a way similar to the microwave-induced Rabi oscillations, the electron in the right dot can be detected as a current, which is proportional to the probability of finding an electron in the right dot, $P_r(t_p)$. This is the projection of the quantum state in the Bloch sphere onto the z-axis, and is given by

$$P_{l/r}(t_p) = \frac{1}{2}[1 \pm \cos(2T_c t_p)] \tag{19}$$

at $\varepsilon_1 = 0$.

Figure 7 shows the coherent oscillation pattern in the $t_p - \varepsilon_1$ plane. As $|\varepsilon_1|$ grows larger, the oscillation amplitude and the oscillation period decrease. For $\varepsilon_1 \neq 0$, the Hamiltonian of Eq. 18 contains an additional fictitious magnetic field in z directions. The pseudo-spin rotates about the direction of the total fictitious magnetic field, which is illustrated in the trajectories in Figs. 7(d)-(f). It is important that any position (state) in the Bloch sphere can be prepared by adjusting ε_1 and t_p in a single pulse. By using a fast pulse generator with a rise time of 50 - 60 ps, successful charge oscillations have been observed in superconducting charge states in a single Cooper-pair box [58, 59], and more recently in single electron states in a double quantum dot [60].

Another important coherent oscillation is the electron-spin resonance, in which the real electron-spin precesses in the presence of a static magnetic field, B_0, in the z direction and an oscillating magnetic field, B_1, in the x direction. The Hamiltonian of the system is given by

$$H(t) = -\tfrac{1}{2}\mu_s(B_0\sigma_z + B_1\cos\omega t\ \sigma_x), \tag{20}$$

which is similar to Eq. 13 by exchanging x and z directions. When the frequency of the oscillating magnetic field is adjusted at the Zeeman splitting energy, the spin direction goes up and down with a precession about z-direction. This is known as the electron-spin resonance, and many kinds of coherent effects have been investigated in many systems. However, because of insufficient measurement sensitivity for electron spin, the electron spin resonance has to be obtained from an ensemble of many spins. Dynamical measurements on a single electron spin are desired (See Sec. 4.3).

3.8 Decoherence in quantum dots

Loss of coherence, which arises from the interaction between a quantum system and the environment, kills the coherent oscillations of the quantum system. There are two or three characteristic times to describe the coherency. Longitudinal relaxation time, which is often called as T_1, is the characterisctic time by which energy of the system is dissipated into the environment (dissipation). The transverse relaxation time, T_2, is the time by which the phase of the system becomes uncertain (decoherence). If the transverse relaxation time originates from the inhomogenity of an ensemble of the quantum system, it is often referred to as T_2^* (dephasing). Since dissipation also kills the phase information, generally $T_2^* \leq T_2 \leq 2T_1$.

Electrons in a quantum dot have orbital and spin degrees of freedom. These degrees of freedom are actually influenced by the environment surrounding the quantum dot, such as photons in the electrical leads and vacuum, phonons of the crystal lattice, other electrons in the electrodes and impurities, nuclear spin of the crystal, and

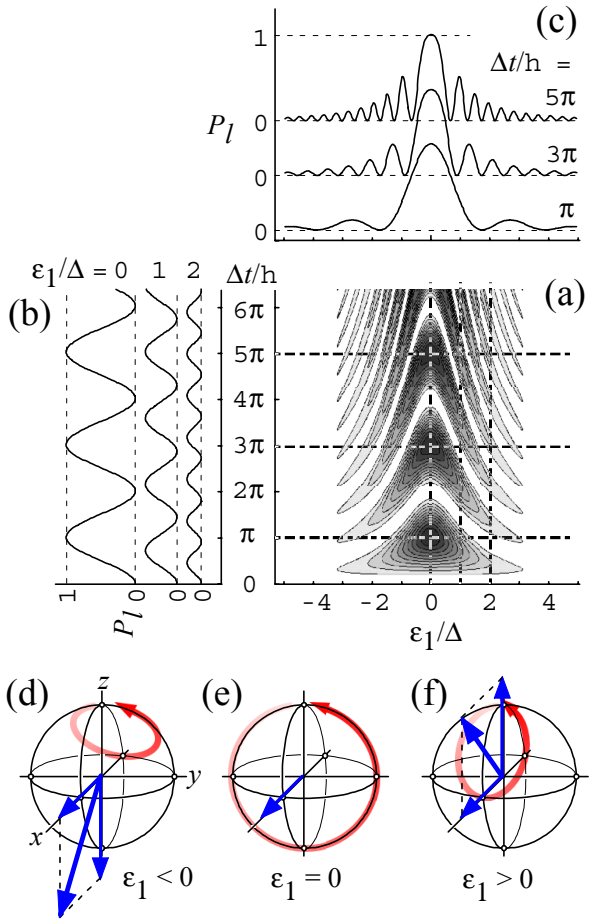

FIG. 7: Time evolution of the two-level system in a double quantum dot. (a) Probability of finding the system in the excited state, P_e (white for 0 and black for 1) as a function of the normalized time, $\Delta t/\hbar$, and the normalized offset energy, ε_1/Δ. (b) Oscillations in the time domain appear at $\varepsilon_1/\Delta = 0$, 1, and 2 (They are offset for clarity). (c) The interference fringe in the offset energy for $\Delta t/\hbar = \pi$, 3π, and 5π. (d-f) Schematic trajectories of the oscillation in the Bloch sphere for (d) $\varepsilon_1 < 0$, (e) $\varepsilon_1 = 0$, and (f) $\varepsilon_1 > 0$.

noise and other fluctuations in the control signal. Moreover, spin and orbital degrees of freedom are coupled with relativistic correction (spin-orbit interactions). The quantum system has to be well isolated from the environment to maintain the coherency of the system.

The characteristic times (T_2^*, T_2 and T_1) of a system depend on the material, devices, measurements, and their parameters. In the next few subsections, we describe some dissipation and dephasing mechanisms that appear in single-electron system.

3.9 Momentum relaxation in a single quantum dot

We start from the energy relaxation process from an excited state to the ground state of a single quantum dot without changing spin. The dominant interaction in this case is the coupling with acoustic phonons for a typical quantum dot whose energy spacing is less than ∼10 meV. Because of the discrete energy states in a quantum dot, the quantum dot only couples with a phonon whose energy is identical to the energy difference of the ground and excited states. At very low temperature, where no phonons are excited, only spontaneous emission of a phonon is important. It should be noted that the wavelength of the phonon can be close to the size of the QDs. This is a notable difference when compared to electron-photon coupling, in which wavelength of the photon is usually much longer than the size of the system. The strength of electron-phonon interaction becomes maximum when the half wavelength is about the size of the quantum dot [61, 62].

We have to consider different types electron-phonon couplings to fully understand the mechanisms. In addition to the normal bulk phonon modes, surface acoustic waves have to be taken into account if the quantum dot is close to the surface within the phonon wavelength, and interface phonon modes if it is close to the interfaces. Moreover, for polar semiconductors, e.g., GaAs, there are two types of couplings. One is the deformation type, in which the deformation of the lattice shifts the potential for electrons, and the other is the piezoelectric type, in which the deformation gives an electric field. Generally, the piezoelectric-type coupling is more efficient for low energy phonons (less than ∼1 meV for GaAs).

The electron-phonon interactions for optical characteristics are intensively studied because inefficient optical properties (the phonon bottleneck effect) are expected for a QD whose energy spacing is relatively large [63]. The phonon bottleneck effect is undesirable with respect to optical characteristics, but it is desired in order to reduce the decoherence of the quantum system. The energy relaxation time is expected to become significantly long, if the energy spacing is not right at the optical phonon energy, and if the corresponding phonon wavelength is longer than the size of the QDs. There are still many questions about its influence on the efficiency of the lu-

minescence, but recent studies indicate that the phonon bottleneck effect does exist when other relaxation mechanisms, which may be related to holes or other electrons, are well suppressed [64–66]. Optical techniques are often restricted by their generated electron-hole pairs, which open other relaxation channels.

As for the transport measurement, in which no holes are generated, the suppression of phonon emission appears more clearly. Excitation spectra in single-electron tunneling characteristics indicate relatively long relaxation time; however, conventional transport characteristics do not give quantitative information about the relaxation time [67]. The recent discovery of time-dependent transport through a QD in the Coulomb blockade regime allows us to measure the energy relaxation time in a QD that contains just one electron (artificial hydrogen atom). The energy relaxation process from the 2p orbital (the 1st excited state) to the 1s orbital (the ground state) is schematically shown in Fig. 8(a). The relaxation time, T_1 = 3 - 10 ns, slightly increases with increasing energy spacing (1.5 - 2.5 meV) by changing the magnetic field (B = 0 - 5 T) [68]. This behavior is understood as the spontaneous emission of an acoustic phonon, and indicates the phonon bottleneck effect. It should be noted that the observed T_1 time is close to the minimum condition, where the half wavelength is about the size of the quantum dot (maximized electron-phonon interaction). The strength of electron-phonon coupling could be reduced by tailoring the structure of the quantum dot.

3.10 Spin relaxation in a quantum dot

When the energy relaxation involves a spin-flip, simple photon or phonon emission cannot contribute to the relaxation. Spin-flip mechanisms, such as spin-orbit or hyperfine interactions, have to be considered together with the phonon emission that is required for energy conservation. Spin-orbit interaction, which mixes the spin and orbital degrees of freedom, is known to be a dominant spin-flip mechanism in 2D electron system in semiconductors. Causes of spin-orbit interaction include the lack of crystal inversion symmetry, the electric field of the confinement potential, and impurities and interfaces of the structures. However, the spin-orbit interaction does not contribute to the spin relaxation in a QD to the first order if the energy spacing is much larger than the spin-orbit induced spin splitting energy (a few μeV for GaAs). Higher-order spin-orbit interactions give rise to a small effect on the spin-flip energy relaxation, whose relaxation time is expected to be longer than 1 ms for a typical GaAs QD [69–72]. Nevertheless, spin-orbit coupling is theoretically predicted to be a major source of the spin-flip energy relaxation process.

The spin-flip energy relaxation time has also been intensively studied in optical measurements. However, the observed relaxation time strongly depends on the exci-

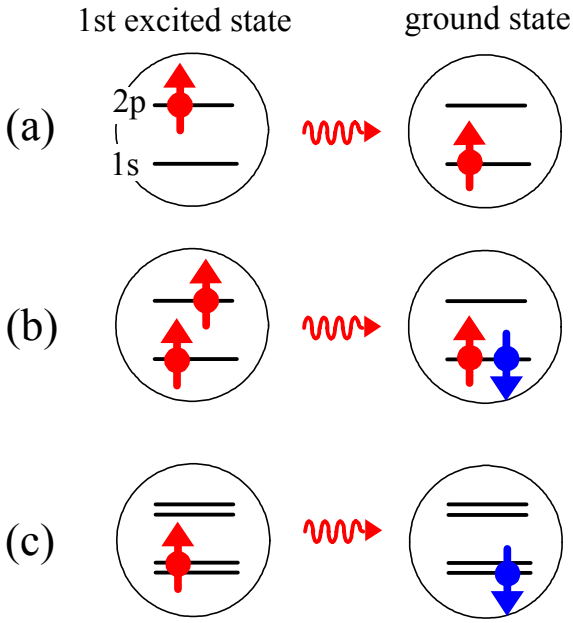

FIG. 8: Energy relaxation processes in a quantum dot. The upper and lower horizontal lines in each circle represents the 2p and 1s orbital states, respectively, in a quantum dot. (a) Momentum relaxation from 2p state to 1s state. (b) Spin and momentum relaxation in two-electron quantum dot. (c) Spin relaxation in one-electron quantum dot. The double line indicates Zeeman splitting in a magnetic field.

tation conditions. When the QD is excited resonantly, a very long relaxation time (>> 20 ns, which is even longer than the experimental limit of the optical technique) has been reported at low temperatures (< 20 K) [73, 74]. However, it is not as long as the theoretical predictions. The optical measurement is restricted by its electron-hole recombination lifetime.

Single electron transport measurements with time-dependent gate voltage allow us to measure extremely long relaxation times (electrical pump and probe technique) [68, 75, 76]. The energy relaxation from the spin triplet state to the spin singlet state in a two-electron quantum dot (artificial helium atom) involves a spin-flip, as schematically shown in Fig. 8(b). This inelastic spin relaxation time is found to be about 200 μs for a specific device. From a detailed analysis, this relaxation was found to be dominated by the co-tunneling process, which exchanges the spin and the energy with the electrode [68]. For instance, a spin-up electron leaves the dot, and simultaneously a spin-down electron enters it. During this process, the QD loses energy and the electrode gains the same energy. Since the strength of the co-tunneling process is determined by the tunneling rate, the co-tunneling process can be easily reduced by increasing the tunneling barrier. Then, the resulting relaxation time should become longer than 200 μs, and may be dominated by spin-orbit interactions.

The inelastic spin relaxation time (> 200 μs) is more than five orders of magnitude longer than when no spin flip is involved (∼10 ns) [68]. The ratio of the relaxation time can be larger than 3×10^4, which is close to the theoretical expectation of 5×10^5 for this structure [70]. It is interesting to compare this ratio to that of real atoms. Quantum dots, or artificial atoms, couple to lattice vibration modes (phonons), while real atoms couple to electromagnetic fields (photons). The strength of the optical transition in real atoms strongly depends on the characteristics of the state, known as selection rules [77]. Typical transition lifetime, or relaxation time, of allowed transitions for electric dipole coupling is on the order of nanoseconds, e.g., 1.6 ns for the Lyman α transition line from the 2p state to the 1s state in a hydrogen atom. However, some transitions have an extremely long relaxation time, e.g., 7860 s for the relaxation from the two-electron spin-triplet excited state to the spin-singlet ground state in a helium atom. In this case, the transition is forbidden by spin conservation and parity [77]. The huge ratio of the relaxation times, more than 10^{12}, for hydrogen and helium atoms, indicates the high quality of the quantum numbers, spin and angular momentum. The ratio decreases with increasing atomic number, because spin-orbit interaction increases and the Russel-Saunders approximation becomes worse. The ratio in a GaAs artificial atom is $>3\times10^4$, which is comparable to the ratio of 10^5 for potassium and calcium atoms, which are located in the same row as the gallium and arsenide in the periodic table. This crude comparison implies that the spin-orbit interaction in the nanostructure is almost comparable to the atomic property.

Another important spin relaxation process is the transition between Zeeman sub-levels in a magnetic field [See Fig. 8(c)]. This relaxation time has not yet been measured with the electrical method, because Zeeman splitting in GaAs QDs is often unresolved in single electron transport measurements. However, this spin relaxation time is expected to be longer than 1 ms, based on consideration of only the spin-orbit interaction [68].

The long spin relaxation time in quantum dots gives rise to spin-dependent tunneling. Since an electron has spin 1/2, a single-electron tunneling changes the total spin of the dot by 1/2. Other tunneling transitions that change the total spin by more than 1/2 should be blocked (spin blockade) [78, 79]. Moreover, the long spin relaxation time induces non-equilibrium transport that cannot be explained by the orthodox CB theory [9, 80].

3.11 Energy relaxation in a double quantum dot

In contrast to single dots, the energy states in a double quantum dot are spatially separated. Here we discuss the energy relaxation between the two charge states in the double dot defined in Sec. 2.5. Suppose two quantum dots are weakly coupled by a tunneling barrier, and consider an energy relaxation between two localized states, i.e. $\varepsilon \gg T_c$. By changing ε, the overlap of the wavefunctions can be modified, as schematically shown in Fig. 4(b)-(d). The transition rate, W, is given by $W = (T_c/\varepsilon)^2 J(\varepsilon)$, where $J(\varepsilon)$ is a spectral function that describes the interaction with its environment. As is the case for momentum relaxation in a single quantum dot, the energy relaxation without spin-flip is dominated by electron-phonon interactions. In the double quantum dot case, the spectral function can be studied by changing ε.

In single-electron transport measurements through a weakly coupled double quantum dot in a series configuration, the current through the device, I, can be directly related to the transition rate, i.e., $I = eW$ for $\varepsilon > T_c$, if the outer tunneling barriers are made more transparent than the inelastic transition of interest [81, 82]. Measurements on GaAs double quantum dots indicate a spectral function close to the ohmic interaction in this system. Because of the relatively small energy (ε = 4 - 100 μeV), piezoelectric interactions with acoustic phonons are the dominant mechanisms.

In some cases, $J(\varepsilon)$ in a double quantum dot shows some structures, which come from the relation between the phonon wavelength and the spacing between the dots [81, 82]. The phonon emission between the two states is enhanced when the spacing is half of the phonon wavelength, but suppressed when the spacing equals the wavelength. The lectron-phonon interaction might be strong to renormalize the single electron tunneling [83]. Even though there is no confinement of phonons, such an oscillatory behavior is observable in the current spectrum

of a double quantum dot.

3.12 Decoherence of a double quantum dot

In contrast to the energy relaxation processes, decoherence is a loss of phase information over the ensemble of measurements. In the discussions of coherent oscillations in the time domain (See Sec. 3.7), we completely neglect the decoherence and dissipation. However, in reality, oscillation does not continue forever, but is dampened over a duration characterized by the decoherence time, T_2. It is convenient to assume an exponential decay of the oscillation amplitude, but the amplitude can decay in a Gaussian shape in some cases [84].

The decoherence of the two-level system in a double quantum dot may be dominated by fluctuations of ε and T_c. The fluctuation changes the frequency of the coherent oscillations, and smears out the oscillation in the ensemble measurement. According to a detailed study of coherent oscillations in superconducting charge states, the $1/f$ noise in the background charge fluctuations is the decoherence mechanism [84]. Although the power spectrum decreases with a $1/f$ dependence at higher frequency, the integrated contributions come from a wide frequency range. A single-electron state has the advantage of high controllability, but this means that it can easily couple to the environment. The mechanism of the charge fluctuations is not well understood, and the reduction of the noise may not be easy.

One way to avoid the influence of fluctuations is to design the quantum state to be less sensitive to. As seen in Fig. 4(a), the energy spacing between two eigenstates is insensitive to the fluctuation of ε at $\varepsilon = 0$ to the first order, while it is sensitive at $\varepsilon > T_c$. Therefore, longer decoherence time is expected at $\varepsilon = 0$. In a superconducting island with a SQUID interferometer to control the Josephson coupling (equivalent to T_c), the quantum system can be set at the saddle point where the energy spacing is insensitive to the fluctuation of ε and T_c. A very long decoherence time of a few μs as compared to the precession period of $\sim$50 ps has been realized [85].

3.13 Radio-frequency single-electron transistor

The single-electron transistor is known to work as a highly sensitive electrometer. In principle, operating frequency can go beyond 1 GHz, if it is determined by the intrinsic RC time-constant of the tunneling resistance and capacitance. However, practical operating frequency is limited to a low frequency range (a few kHz at most) in conventional dc current measurements. The capacitance of the electrodes, including the measurement instruments, is so large that the frequency range is restricted by the RC time constant of the electrode capacitance and the tunneling resistance.

The radio-frequency single-electron transistor (RF-SET), which works as a wide-band and highly sensitive electrometer, is a SET combined with an impedance transformer (LC resonator) [86]. The capacitance of the problem can be canceled by an external inductor located close to the SET device, if it is operated at the resonant frequency, f_{res}. The maximum frequency of the RFSET is approximately given by f_{res}/Q_{LC}, where Q_{LC} is the quality factor of the resonator. The external LC resonator placed close to an SET device has a typical bandwidth of about 100 MHz with $f_{res} \sim 1$ GHz and $Q_{LC} \sim 10$. Better performance (higher f_{res} and larger Q_{LC}) may be obtained using an on-chip resonator. The conductance of the SET is measured by the reflection or the transmission of the rf carrier signal at f_{res} [87, 89]. The transmission amplitude, or the small change in the reflected signal, is, in principle, proportional to the admittance (the inverse of the impedance) of the SET [89].

The sensitivity of a charge respective to the island can be about 10^{-5} e/$\sqrt{Hz}$, which is usually restricted by the noise of the high-frequency amplifier. This means that the intrinsic noise of the RFSET (shot noise) is very low at high frequency ($>$ 10 kHz), while it suffers from 1/f noise at low frequency. Theoretically, the noise of the RFSET is expected to be very close to that of the conventional SET [88]. The charge sensitivity can be as low as 2×10^{-6} e/$\sqrt{Hz}$ for an optimized device using a practical superconducting island, and better sensitivity is expected by using a smaller island [86].

The RFSET technique is very attractive, and can be used as high-sensitive fast-response electrometer for many applications [90]. If the RFSET is attached to another quantum dot located in another conductive channel, each single-electron tunneling process would be detected with a high sensitivity. This would be an extremely sensitive current meter, in which current flow could be detected by counting tunneling electrons. If a RFSET is attached to a two-level system in a double quantum dot (See Sec. 2.5 and 3.7), the charge state can be detected in a short time [91]. This is desirable for further investigation of quantum dynamics and correlations in single electron systems.

4. TOWARD QUANTUM INFORMATION PROCESSING

Quantum information processing is digital data processing with the aid of coherent time-evolution of quantum states. Analogous to a bit that is the unit of digital information, the unit of quantum information is the quantum bit (qubit), which is basically realized in any single two-level system. Quantum information processing would provide various advantages that have never been obtained in the conventional classical approach [92, 93]. For instance, quantum cryptography would provide secure telecommunications because any unknown single

quantum state cannot be duplicated and because any unknown single quantum state cannot be determined completely. Quantum non-demolition measurement scheme improves the measurement accuracy by avoiding back action. Quantum computation is programmable interferometry, in which only one or a few desired answers can be efficiently obtained from an extremely large number of candidates. Recently, quantum information processing has become attractive for realizing very specific tasks.

4.1 Concept of quantum computation

First, we stress that quantum information processing is completely different from so-called 'quantum devices'. Quantum devices are designed to transform a classical input, like a voltage, into another classical output, like a current, with excellent transfer characteristics with the aid of quantum mechanics. The resonant tunneling diode, which is a typical quantum device that works even at room temperature, shows negative differential resistance in the current (output) - voltage (input) characteristics. Although quantum mechanics is required to design the diode, one can use the diode without considering the quantum mechanics, if the characteristics are known. In quantum information processing, however, the quantum state is the carrier of information. The quantum state is transformed from an input state to an output state by applying an external field, e.g., an electromagnetic field, in a certain period. The transformation of the quantum state is called a quantum logic gate, and should be a unitary transformation to keep coherency. The quantum state changes by applying a series of quantum logic gates necessary for quantum computation from the beginning, at which some classical values are input to the quantum state, till the end of the computation, at which the output states are finally measured as classical values. One may not measure the intermediate state, which would result in the collapse of the quantum state. Quantum computing requires a high degree of quantum coherence for a long enough time to complete the computation.

In principle, any calculation that can be performed in a conventional classical computer can also be performed in a quantum computer. But this is not a good idea, because quantum computation requires extremely high accuracy and coherency in the quantum logic gates, and because computation errors are unavoidable. However, one can design the algorithm of quantum computation in such a way that a series of data processings are performed at once in a parallel fashion (quantum parallelism). Then, quantum computation is expected to provide extremely *efficient* calculations for specific problems that cannot be solved *efficiently* with conventional classical computers. For instance, factorization of a large number is a formidable task for conventional computers. There are no efficient algorithms for this in classical computers, and one has to check sequentially whether the number to factorize is divisible by a number from 2 to the square root of the number to factorize (Actually, there is a better way using a probabilistic algorithm). Nevertheless, factorization of a 1000 digit number would require 10^{25} years (longer than the history of the universe) by using 1000 workstations in parallel [94]. In Shor's factoring algorithm for quantum computing, the factorization problem is attributed to how efficiently a Fourier transformation is calculated. The quantum Fourier transform can be constructed from a few kinds of quantum logic gates, and can be calculated very efficiently. Factoring a 1000 digit number would require only a few 10^6 steps in the quantum computation [94]. The factorization (quantum Fourier transformation) is just an example of quantum computation. There are many algorithms, such as database search and quantum simulations, that would solve some problems very *efficiently*.

Although the potential of quantum computing is fascinating, only a few small-scale quantum computers have been realized. The solution nuclear-magnetic-resonance (NMR) quantum computer is the most advanced quantum computer. The nuclear spin of an atom is used as a qubit, and a single molecule that contains distinguishable atoms (nuclear spins) works as a quantum computer. The NMR quantum computer works by applying a sequence of radio frequencies (quantum logic gates) to many molecules (quantum computers) in a solution. Recently, factorization of 15, whose prime numbers are 3 and 5, was demonstrated using a solution NMR QC with 7 qubits [95]. However, the solution NMR QC has problems integrating large numbers of qubits, and thus may not be a practical quantum computer. It is generally accepted that solid-state quantum computers are good candidates for scalability. There are many proposals based on the charge state or flux state in a superconducting island, charge state, electron-spin state, or exciton state (electron-hole pair) in a semiconductor quantum dot, nuclear-spin state of impurities or crystals. One-qubit operations have been demonstrated in some of solid-state systems, and two-qubit operations should be achieved in the near future.

To construct a quantum computer, single quantum states would have to be prepared physically, manipulated coherently, preserved for a long enough time, measured individually, and integrated in a large quantity [96]. Each these points requires further development. Decoherence is one of the major problems in solid-state systems. Fundamental research has been conducted to reduce the decoherence problems and to devise the best quantum logic gates. In the following two subsections, we briefly summarize the strategies for realizing quantum computers using *single-electron dynamics*.

4.2 Single-electron charge qubit

As we discussed in Sec. 2.5, a single electron in a double quantum dot can be used as a two-level system, serving as a qubit (charge qubit) [18, 97]. A similar charge qubit has been realized in a superconducting island, in which the two-level system is represented by an extra Cooper pair occupying or not occupying the island (superconducting charge qubit). The coherent oscillations induced by microwave irradiation or by a high-speed voltage pulse can be used as a rotation gate for one-qubit operation (Sec. 3.7). The qubit state can be controlled to any state [θ and ϕ in the Bloch sphere, see Fig. 7(d)-(f)] by tailoring the pulse shape. The NOT gate, which reverses the classical information, can be obtained by applying a π pulse (a half cycle of the oscillation at $\varepsilon = 0$). The Hadamard gate, which creates a superposition state from an eigenstate, is achieved by a $\pi/2$ pulse (a quarter cycle of the oscillation).

When two sets of double quantum dots (two qubits) are fabricated to couple electrostatically, any superposition of four bases $|00\rangle$, $|01\rangle$, $|10\rangle$, and $|11\rangle$, where first and second numbers indicate the location of electron in respective double dot, can be prepared. The dipole coupling between the two qubits affects the total energy of the states. The controlled-NOT gate, which is a typical two-qubit operation, can be performed by applying a voltage pulse to degenerate two states, say $|00\rangle$ and $|01\rangle$, for a certain period that exchanges the two states. This means that the state of the second qubit (target qubit) is reversed (NOT operation) only when the first qubit (control qubit) is 0. If this is performed coherently, the controlled-NOT gate should work for any superposition state as well. For instance, starting from the initial state $|00\rangle$, the Hadamard gate on the fist qubit followed by the controlled-NOT gate brings an entangled state

$$|00\rangle \rightarrow_H |00\rangle + |10\rangle \rightarrow_{CNOT} |01\rangle + |10\rangle, \qquad (21)$$

in which the first and second qubits are correlated [93].

The qubit state can be measured by an electrical current as explained in Sec. 3.7. In this case, ensemble averaging over many measurements are required due to small current sensitivity. In some cases, for example when the correlation between the two qubits is essential, it is desirable to measure a single qubit state without any ensemble averaging. The RF-SET technique discussed in Sec. 3.13 would provide a single-shot measurement without averaging for the charge qubit. If the electrostatic coupling between the qubit and the RFSET can be made sufficiently large, the qubit state can be measured in a relatively short time (hopefully ∼10 ns). Of course, the RFSET can be turned off by switching off the carrier rf signal during the quantum computation to minimize the decoherence from the measurement.

4.3 Single-electron spin qubit

The spin degree of freedom is an alternative way to construct a qubit [98]. If the charge qubit is an artificial qubit, electron spin is a natural qubit. The coherency and manipulation of electron spins have been studied in many systems. The spin coherence time of conductive electrons in bulk GaAs crystal can be longer than 100 ns [99], and electron spin bound to a donor in silicon shows $T_2 \sim 300$ μs [100]. Electron-spin based quantum computation is motivated by the long decoherence time. However, in contrast to the countless studies on the ensemble of spins, little work has been done on the manipulation of single-electron spin. In order to address each electron spin (qubit) in a quantum computer, single-spin manipulation and measurement techniques are essential.

A simple scheme for one-qubit operation is the electron spin resonance discussed in Sec. 3.7. The effective g-factor of each electron spin can be made different for different quantum dots by using g-factor engineering, so that each qubit is addressed by a corresponding microwave frequency [98]. Or a moderate magnetic field gradient in the device may be useful in changing the Zeeman splitting energy. However, a typical one-qubit operation using an electron spin resonance will require a relatively long time, ∼100 ns, because of the weak magnetic dipole transition. Alternative ways using the optical Stark effect in a specific band structure [101] or exchange coupling among three electron spins constituting one qubit [102] are promising for much faster operations. Two-qubit operation can also be performed by the exchange coupling between two quantum dots [103].

Single-shot spin measurement is a challenging technique for quantum information technology. One proposal is based on the spin-dependent tunneling between two quantum dots combined with an RFSET [104]. When each of the two quantum dots possesses one electron spin before the measurement, tunneling from one dot to the other is allowed, if the two electron spins can make a spin pair (spin singlet state) [105]. This spin-dependent tunneling could be measured with an RFSET in a short time.

ACKNOWLEDGMENTS

Discussions with R. Aguado, D. G. Austing, H. D. Cheong, T. Hayashi, Y. Hirayama, T. Honda, K. Ishibashi, T. Itakura, A. V. Khaetskii, L. P. Kouwenhoven, G. Lang, Y. Nakamura, T. H. Oosterkamp, S. Tarucha, Y. Tokura, W. G. van der Wiel, are gratefully acknowledged.

=== Glossary ===

Adiabatic approximation: When the Hamiltonian of a quantum system changes slowly, the wavefunction can be approximated by an eigenstate of

the instantaneous Hamiltonian (adiabatic approximation). However, when the Hamiltonian changes very fast (non-adiabatically), the wave-function becomes a non-stationary superposition state.

Bloch sphere: Any linear superposition of two orthonormal bases can be expressed in a form, Eq. 4, which indicates a point on the unit sphere (Bloch sphere). This representation is very useful for visualizing a quantum state.

Cotunneling: Cotunneling is two or more tunneling processes that occur successively in a short time. The intermediate state may have a high energy, if the energy cost is within the energy uncertainty given by the interval of the corresponding tunneling processes.

Coulomb interaction: Coulomb interaction between two or more electrons can be described by direct integral, which comes from the direct overlap of the two wavefunctions, and exchange integral, which depends on the spin state.

Poisson statistics: Poisson statistics is a frequency distribution when the probability of an event is very small. The probability for n events happening is given by $p(n) = a^{-n}e^{-a}/n!$, where a is the average number of the events. When the distribution is narrower than the Poisson statistics, it is called sub-Poisson statistics.

Rabi oscillation: When a coherent electromagnetic field is resonantly applied to a two-level system, emission and absorption takes place coherently and oscillatory (Rabi oscillation).

Spontaneous/stimulated emission: When a transition from a higher-energy state to a lower-energy state occurs by an emission of a boson (photon or phonon), it consists of spontaneous emission, which always occurs due to vacuum fluctuation of the bosonic system, and stimulated emission, which is proportional to the number of existing bonons.

1/f noise: 1/f noise has a power spectrum close to $1/f$ frequency dependence. In electrical noise, the $1/f$ noise comes from ensemble of many electron traps, each of which emit or capture an electron independently (Poisson statistics).

REFERENCES

[1] H. Grabert and M. H. Devoret (Eds.), *Single Charge Tunneling, Coulomb Blockade Phenomena in Nanostuctures*, NATO ASI series B 294, Plenum Press, New York (1991).

[2] L. P. Kouwenhoven, C. M. Marcus, P. L. McEuen, S. Tarucha, R. M. Westervelt, and N. S. Wingreen, in *Mesoscopic Electron Transport* edited L. L. Sohn, L. P. Kouwenhoven, and G. Schön, NATO ASI series E 345, Kluwer Academic, Dordrecht (1997), pp. 105-214.

[3] U. Meirav, M. A. Kastner, and S. J. Wind, Phys. Rev. Lett. 65, 771 (1990).

[4] T. Fujisawa and S. Tarucha, Appl. Phys. Lett. **68**, 526 (1996).

[5] D. G. Austing, T. Honda, and S. Tarucha, Semicond. Sci. Tecnol. **11**, 212 (1996).

[6] T. A. Fulton and G. J. Dolan, Phys. Rev. Lett. **59**, 109 (1987).

[7] Y. Nakamura, C. D. Chen, J. S. Tsai, Jpn. J. Appl. Phys. **35**, L1465 (1996).

[8] D. G. Austing, S. Tarucha, P. C. Main, M. Henini, S. T. Stoddart, and L. Eaves, Appl. Phys. Lett. 75, 671 (1999).

[9] T. Fujisawa, D. G. Austing, Y. Tokura, Y. Hirayama, and S. Tarucha, Phys. Rev. Lett. 88, 236802 (2002).

[10] L. P. Kouwenhoven, D. G. Austing, and S. Tarucha, Reports on Progress in Physics **64**, 701 (2001).

[11] S. Tarucha, D. G. Austing, T. Honda, R. J. van der Hage and L. P. Kouwenhoven, Phys. Rev. Lett. **77**, 3613 (1996).

[12] L. P. Kouwenhoven, T. H. Oosterkamp, M. W. S. Danoesastro, M. Eto, D. G. Austing, T. Honda, and S. Tarucha, Science **278**, 1788 (1997).

[13] F. R. Waugh, M. J. Berry, D. J. Mar, R. M. Westervelt, K. L. Campman, and A. C. Gossard, Phys. Rev. Lett. 75, 705 (1995).

[14] C. Livermore, C. H. Crouch, R. M. Westervelt, K. L. Campman, and A. C. Gossard, Science 274, 1332 (1996).

[15] N. C. van der Vaart, S. F. Godijn, Yu. V. Nazarov, C. J. P. M. Harmans, and J. E. Mooij, Phys. Rev. Lett. **74**, 4702 (1995).

[16] W. G. van der Wiel, S. De Franceschi, J. M. Elzerman, T. Fujisawa, S. Tarucha, L. P. Kouwenhoven, Rev. Mod. Phys (in press).

[17] L. P. Kouwenhoven, Science 268, 1440 (1995).

[18] T. H. Oosterkamp, T. Fujisawa, W. G. van der Wiel, K. Ishibashi, R. V. Hijman, S. Tarucha, and L. P. Kouwenhoven,Nature 395, 873 (1998).

[19] R. H. Blick, D. Pfannkuche, R. J. Haug, K. v. Klitzing, and K. Ebel, Phys. Rev. Lett. 80, 4032 (1998).

[20] D. Esteve, in "*Single Charge Tunneling, Coulomb Blockade Phenomena in Nanostuctures*" ed. H. Grabert and M. H. Devoret, NATO ASI series B 294 (Plenum Press, New York, 1991), pp. 109-137.

[21] K. K. Likharev and A. B. Zorin, J. Low Temp. Phys. 59, 347 (1985).

[22] L. J. Geerling, V. F. Anderegg, P. A. M. Holweg, J. E. Mooij, H. Pothier, D. Esteve, C. Urbina, and M. H. Devoret, Phys. Rev. Lett. 64, 2691 (1990).

[23] H. Pothier, P. Lafarge, C. Urbina, D. Esteve, and M. H. Devoret, Europhys. Lett. 17, 249 (1992).

[24] D. V. Averin and Yu. V. Nazarov, in "*Single Charge Tunneling, Coulomb Blockade Phenomena in Nanostuctures*" ed. H. Grabert and M. H. Devoret, NATO ASI series B 294 (Plenum Press, New York, 1991), pp. 217-248.

[25] M. W. Keller, J. M. Martinis, and R. L. Kautz, Phys. Rev. Lett. 80, 4530 (1998).

[26] M. W. Keller, J. M. Martinis, A. H. Steinbach, and N. M. Zimmerman, IEEE Trans. Instrumentation and Measurement, 46, 307 (1997).

[27] D. V. Averin, and K. K. Likharev, J. Low. Temp. Phys. 62, 345 (1986).

[28] A. B. Zorin, S. V. Lotkhov, H. Zangerle, and J. Niemeyer, J. Appl. Phys. 88, 2665 (2000).

[29] P. Delsing, K. K. Likharev, L. S. Kuzmin, and T. Claeson, Phys. Rev. Lett. 63, 1861 (1989).

[30] S. Hershfield, J. H. Davis, P. Hyldgaard, C. J. Stanton, and J. W. Wilkins, Phys. Rev. B 47, 1967 (1993).

[31] H. Birk, M. J. M. de Jong, and C. Schönenberger, Phys. Rev. Lett. 75, 1610 (1995).

[32] M. S. Choi, F. Plastina, R. Fazio, Phys. Rev. Lett. 87, 116601 (2001).

[33] Q. Niu, Phys. Rev. Lett. 64, 1812 (1990).

[34] V. I. Talyanskii, J. M. Shilton, M. Pepper, C. G. Smith, C. J. B. Ford, E. H. Linfield, D. A. Ritchie, and G. A. C. Jones, Phys. Rev. B 56, 15180 (1997).

[35] J. Cunningham, V. I. Talyanskii, J. M. Shilton, M. Pepper, M. Y. Simmons, and D. A. Ritchie, Phys. Rev. B 60, 4850 (2000).

[36] J. Cunningham, V. I. Talyanskii, J. M. Shilton, and M. Pepper, Phys. Rev. B 62, 1564 (2000).

[37] T. J. M. M. Janssen and A. Hartland, Physica B 284-288, 1790 (2000).

[38] P. A. Maksym, Phys. Rev. B 61, 4727 (2000).

[39] P. K. Tien and J. P. Gordon, Phys. Rev. 129, 647 (1963).

[40] J. R. Tucker, M. J. Feldman, Rev. Mod. Phys. 57, 1055 (1985).

[41] J. M. Hergenrother, M. T. Tuominen, J. G. Lu, D. C. Ralph, M. Tinkham, Physica B 203, 327 (1994).

[42] B. J. Keay, S. Zeuner, S. J. Allen Jr., K. D. Maranowski, A. C. Gossard, U. Bhattacharya, and M. J. W. Rodwell, Phys. Rev. Lett. 75, 4102 (1995).

[43] S. Verghese, R. A. Wyss, Th. Schäpers, Q. Hu, A. Förster, and M. J. Rooks, Phys. Rev. B 52, 14834 (1995).

[44] L. P. Kouwehhoven, S. Jauhar, J. Orenstein, P. L. McEuen, Y. Nagamune, J. Motohisa, H. Sakaki, Phys. Rev. Lett. 73, 3443(1994).

[45] R. H. Blick, R. J. Haug, D. W. van der Weide, K. von Klitzing, and K. Eberl, Appl. Phys. Lett. 67, 3924 (1995).

[46] T. H. Oosterkamp, L. P. Kouwehhoven, A. E. A. Koolen, N. C. van der Vaart, and C. J. P. M. Harmans, Phys. Rev. Lett. 78, 1536 (1997).

[47] T. H. Stoof and Yu. V. Nazarov, Phys. Rev. B 53, 1050 (1996).

[48] T. Fujisawa and S. Tarucha, Superlattices and Microstructures 21, 247 (1997).

[49] Y. Nakamura, C. D. Chen, and J. S. Tsai, Phys. Rev. Lett. 79, 2328 (1997).

[50] R. Aguado and L. P. Kouwenhoven, Phys. Rev. Lett. 84, 1986 (2000).

[51] T. Fujisawa and S. Tarucha, Japan. J. Appl. Phys. 36, 4000 (1997).

[52] A. N. Korotkov, D. V. Averin, K. K. Likharev, Phys. Rev. B 49, 7548 (1994).

[53] C. A. Stafford and N. Wingreen, Phys. Rev. Lett. 76, 1916 (1996).

[54] M. Holthaus and D. Hone, Phys. Rev. B 47, 6499 (1993).

[55] W. G. van der Wiel, T. Fujisawa, T. H. Oosterkamp, and L. P. Kouwenhoven, Physica B 272, 31 (1999).

[56] M. Brune, F. Schmidt-Kaler, A. Maali, J. Dreyer, E. Hagley, J. M. Raimond, and S. Haroche, Phys. Rev. Lett. 76, 1800 (1996).

[57] H. Kamada, H. Gotoh, J. Temmyo, T. Takagahara, and H. Ando, Phys. Rev. Lett 87, 246401 (2001).

[58] Y. Nakamura, Yu. A. Pashkin, and J. S. Tsai, Nature 398, 786 (1999).

[59] Y. Nakamura, and J. S. Tsai, J. Low Temp. Phys. 118, 765 (2000).

[60] T. Hayashi, T. Fujisawa, H. D. Cheong, and Y. Hirayama, to be submitted.

[61] U. Bockelmann and G. Bastard, Phys. Rev. B 42, 8947 (1990).

[62] U. Bockelmann, Phys. Rev. B 50, 17271 (1994).

[63] H. Benisty, Phys. Rev. B 51, 13281 (1995).

[64] R. Heitz, H. Born, F. Guffarth, O. Stier, A. Schliwa, A. Hoffmann, and D. Bimberg, Phys. Rev. B 64, 241305 (2001).

[65] J. Urayama, T. B. Norris, J. Singh, and P. Bhattacharya, Phys. Rev. Lett. 86, 4930 (2001).

[66] S. Malik, E. V. Le Ru, D. Childs, and R. Murray, Phys. Rev. B. 63, 155313 (2001).

[67] J. Weis, R. J. Haug, K. v. Klitzing, and K. Ploog, Phys. Rev. Lett. **71**, 4019 (1993).

[68] T. Fujisawa, D. G. Austing, Y. Tokura, Y. Hirayama, and S. Tarucha, Nature 419, 278 (2002).

[69] D. M. Frenkel, Phys. Rev. B 43, 14228 (1991).

[70] A. V. Kaetskii, and Yu. V. Nazarov, Phys. Rev. B 61, 12639 (2000).

[71] A. V. Kaetskii, and Yu. V. Nazarov, Physica E 6, 470 (2000).

[72] S. I. Erlingsson, Yu. V. Nazarov, and V. I. Fal'ko, cond-mat/0104148 (2001).

[73] Y. Toda, S. Shinomori, K. Suzuki, and Y. Arakawa, Phys. Rev. B 58, R10147 (1998).

[74] M. Paillard, X. Marie, P. Renucci, T. Amad, A. Jbeli, J. M. Gerard, Phys. Rev. Lett. 86, 1634 (2001).

[75] T. Fujisawa, Y. Tokura, and Y. Hirayama, Phys. Rev. B **63**, 081304(R) (2001), Physica B **298**, 573 (2001).

[76] T. Fujisawa, Y. Tokura, D. G. Austing, Y. Hirayama, and S. Tarucha, Physica B 314, 224 (2002).

[77] H. A. Bethe, and E. E. Salpeter, *Quantum Mechanics of One- and Two-Electron Atoms*, (Springer, Berlin, 1957).

[78] D. Weinmann,W. Häusler, and B. Kramer., Phys. Rev. Lett **74**, 984 (1995).

[79] M. Ciorga, A. S. Sachrajda, P. Hawrylak, C. Gould, P. Zawadzki, S. Jullian, Y. Feng, and Z. Wasilewski, Phys. Rev. B **61**, R16315 (2000).
[80] O. Agam, N. S. Wingreen, B. L. Altshuler, D. C. Ralph, and M. Tinkham, Phys. Rev. Lett. **78**, 1956 (1997).
[81] T. Fujisawa, T. H. Oosterkamp, W. G. van der Wiel, B. W . Broer, R. Aguado, S. Tarucha, and L. P. Kouwenhoven, Science 282, 932 (1998).
[82] T. Fujisawa, W. G. van der Wiel, L. P. Kouwenhoven, Physica E 7, 413 (2000).
[83] T. Brandes and B. Kramer, Phys. Rev. Lett. 83, 3021 (1999).
[84] Y. Nakamura, Yu. A. Pashkin, T. Yamamoto, and J. S. Tsai, Phys. Rev. Lett. 88, 047901 (2002).
[85] D. Vion, A. Aassime, A. Cottet, P. Joyez, H. Pothier, C. Urbina, D. Esteve, M. H. Devoret, Science, 296, 886 (2002).
[86] R. J. Schoelkopf, P. Wahlgren, A. A. Kozhevnikov, P. Delsing, D. E. Prober, Science, 280, 1238 (1998).
[87] T. Fujisawa and Y. Hirayama, Appl. Phys. Lett. 77, 543 (2000).
[88] A. N. Korotkov and M. A. Paalanen, Appl. Phys. Lett. 74, 4052 (1999).
[89] H. D. Cheong, T. Fujisawa, T. Hayashi, Y. Hirayama, and Y. H. Jeong, Appl. Phys. Lett. 81, 3257 (2002).
[90] M. H. Devoret and R. J. Schoelkopf, Nature 406, 1039 (2000).
[91] A. Aassime, G. Johansson, G. Wendin, R. J. Schoelkopf, and P. Delsing, Phys. Rev. Lett. 86, 3376 (2001).
[92] Eds. D. Bouwmeester, A. Ekert, and A. Zeilinger, The Physics of Quantum Information, (Springer, 2000).
[93] M. A. Nielsen and I. L. Chuang, Quantum Computation and Quantum Information, (Cambridge, 2000).
[94] S. L. Braunstein, Quantum computation: a tutorial, http://chemphys.weizmann.ac.il/~schmuel/comp/comp.html.
[95] L. M. K. Vandersypen, M. Steffen, G. Breyta, C. S. Yannoni, M. H. Sherwood, and I. L. Chuang, Nature 414, 883 (2001).
[96] D. P. DiVincenzo, in *Mesocopic Electron Transport* edited L. L. Sohn, L. P. Kouwenhoven, and G. Schön, NATO ASI series E 345, Kluwer Academic, Dordrecht (1997), pp. 657-677.
[97] A. Barenco, D. Deutsch, A. Ekert, and R. Jozsa, Phys. Rev. Lett. 74, 4083 (1995).
[98] D. Loss and D. P. DiVincenzo, Phys. Rev. A 57, 120 (1998).
[99] J. M. Kikkawa and D. D. Awschalom, Phys. Rev. Lett. 80, 4313 (1998).
[100] M. Chiba and A. Hirai, J. Phys. Soc. Jpn. 33,730 (1972).
[101] J. A. Gupta, R. Knoble, N. Samarth, and D. D. Awschalom, Science 292, 2458 (2001).
[102] D. P. DiVincenzo, D. Bacon, J. Kempe, G. Burkard, and K. B. Whaley, Nature 408, 339 (2000).
[103] G. Burkard, D. Loss and D. P. DiVincenzo, Phys. Rev. B 59, 2070 (1999).
[104] B. E. Kane, N. S. McAlpine, A. S. Dzurak, R. G. Clark, G. J. Milburn, He Bi Sun, and H. Wiseman, Phys. Rev. B 61, 2961 (2000).
[105] K. Ono, D. G. Austing, Y. Tokura, and S. Tarucha, Science 297, 1313 (2002).